Exploring the usage of Time-of-Flight Cameras for contact and remote Photoplethysmography

Caterina Nahler*, Bernhard Feldhofer*, Matthias Ruether†, Gerald Holweg* and Norbert Druml*
*Infineon Technologies Austria AG, Graz, Austria
{caterina.nahler2, bernhard.feldhofer, gerald.holweg, norbert.druml}@infineon.com
†Institute for Computer Graphics and Vision, Graz University of Technology, Austria
{ruether}@icg.tu-graz.ac.at

***Abstract*—The heart beat is one of the basic vital signs, but the pulse wave can communicate much more information than the beat frequency of the heart. Through the heart rate variability (HRV) among other things, stress level and drowsiness can be inferred. Reliable HRV measurements are commonly obtained by electrocardiography (ECG). In this paper we analyse the correlation between HRV and pulse rate variability (PRV) obtained from contact or remote photoplethysmography (PPG) on a Time-of-Flight (ToF) camera from PMD Technologies AG. The ToF camera is independent of passive illumination as it uses an infrared (IR) light source, which is invisible to the human eye. Therefore, potential use cases include driver monitoring or convenient heart rate measurement with smart phones. We will demonstrate methods for using a ToF camera for contact and remote PPG. For contact PPG the sensor is mounted directly on the subjects body. The pulse wave is calculated as the mean amplitude intensity of all pixels. For remote PPG the sensor is mounted to measure the subjects face. The pulse wave cannot be found in every part of exposed skin. Therefore, the part of the skin with the clearest signal is localised and the pulse wave is recovered from there, by means of passband filtering and blind source separation. Our results show that contact PPG on a ToF camera has high accuracy and highly correlates with a commercial IR pulse oximetry device, as well as with an ECG grade chest belt. For remote PPG our method shows correlation with the ToF contact PPG signal.**

***Index Terms*—Time-of-Flight, ToF, remote, contact, photoplethysmography, PPG, rPPG, infrared, pulse, heart beat**

I. Introduction

The standard method for heart rate and vital sign observations is the electrocardiography (ECG). An alternative method is the photoplethysmography (PPG). The blood oxygenation and volume changes affect the light absorption characteristics of living tissue. PPG is based on non-invasive measurement of these light absorption changes. Contact sensors produce a measurement, either by means of reflected or transmitted light, while being loosely attached to the subject's body [1]. Alrick Hertzman first described a setup to photoelectrically measure the blood volume on fingers and toes in 1937 [2]. In contrast to contact PPG, remote PPG relies mostly on reflective measurement. One of the first versions of remote PPG to measure the face was developed in 2008 [3]. Earlier implementations focused the camera on other parts of the human body, such as the arm [4]. Nowadays PPG has already been explored for many applications, including the measurement of blood pressure and oxygenation [4], breathing cycles, mental stress [5], drowsiness detection [6], sleep monitoring and heart rhythm disturbances [7]. A recent area of research includes the usage of contact and remote PPG for driver monitoring [6], [8].

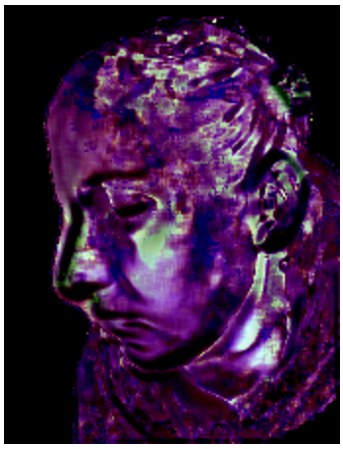

Fig. 1. A visualisation of the pulse wave analysis on the ToF amplitude video data. Every pixel in the video is analysed for the likelihood of containing a clear pulse wave. It can be seen that the carotid artery becomes visible as a bright spot. This indicates, that a clear pulse wave signal is contained in that region.

The Time-of-Flight (ToF) camera is independent of passive illumination as it uses an active infrared (IR) light source, that is invisible to the human eye. The camera, therefore has potential for remote PPG also during night time. Most of the mentioned use cases can benefit from this property. PPG further enables convenient heart rate measurement with smartphones. Remote PPG variants using the front facing camera exist [9]. Recently, remote PPG has also been integrated into augmented reality. An application was developed which uses the HoloLens and RGB data to measure and visualize another human's heart rate [10].

In this paper, we will explore the usage of the Pico Flexx ToF camera from PMD Technologies AG for contact and remote PPG. We contribute two methods which are, subsequently shown, to work on the data provide by the Pico Flexx ToF camera. For contact PPG, the pulse wave is calculated as the mean amplitude intensity of all pixels. For remote PPG the sensor is mounted to measure the subjects face. The pulse wave cannot be found in every part of exposed skin. Therefore, we propose a novel combination approach to select the part of

the skin with the clearest signal. An example visualisation of the signal localisation metrics is shown in Fig. 1. The pulse wave is recovered from the selected skin region, by means of passband filtering and blind source separation. The remainder of the paper is structured as follows. Background information will be provided in Section II. The overview on related work is given in Section III. The method will be described in detail in Section IV and the results including a short discussion will be provided in Section V. A summary of the findings will conclude this paper in Section VI.

II. Background

A. Pulse Measurement

Commonly known ways to measure the heart rate include ECG and PPG. The typical heart beat signal which is known from ECG is not the same as in PPG. The optically measured signal is called a pulse wave. The R-R intervals (peak to peak distances) in ECG measurements are closely correlated with the N-N intervals (peak to peak distances) in PPG. The Heart rate variability (HRV) is one of the most promising markers of the autonomic nervous system. It is the variation of time intervals between successive peaks, obtained from an ECG signal [11]. However, the variation of peak intervals obtained from a PPG signal is the pulse rate variability (PRV). HRV measures were shown to highly correlated with PRV measures [12]–[14]. To evaluate the accuracy of our methods, several measures are extracted from the pulse wave. The average heart rate (AHR) is useful to extrapolate the heart beats up to a minute from a short measurement. For this calculation it is necessary to measure several peaks and calculate the time interval between the peaks. The average value $\overline{\Delta^t}$ is then formed over all the extracted time intervals and with the resulting value a prediction up to a whole minute

$$BPM = \overline{\Delta^t} \cdot 60, \tag{1}$$

where BPM means beats per minute, is possible.

The standard deviation of R-R intervals (SDRR) or respectively N-N intervals (SDNN) can be calculated as

$$SDNN[s] = \sqrt{\frac{1}{M-1} \cdot \sum_{i=1}^{M} (\Delta_i^t - \overline{\Delta^t})^2}, \tag{2}$$

where M is the number of intervals counted in the measurement and Δ_i^t are the time intervals between the peaks [7].

Another measure of the HRV is the coefficient of variation (CV) [7]. In this paper, we are using the CV obtained from the PPG signal (CV_{PRV}) to compare our method with the CV obtained from a Polar H7 (CV_{HRV}) which claims to have ECG quality. We calculate the CV according to the standard equation. Therefore, CV_{PRV} is calculated as

$$CV_{PRV}[\%] = \frac{SDNN[s]}{\overline{\Delta^t}[s]} \cdot 100[\%]. \tag{3}$$

Among other information, it is possible to infer stress level [5], breathing cycles, heart rhythm disturbances [7] and risk for sudden heart failure, from the HRV. These values can only be calculated if the measurement is very accurate. In healthy subjects at rest, HRV measures and PRV measures have a high correlation. However as PPG is quite vulnerable to motion artefacts, the reliability of the PRV measurement under motion is limited in comparison to ECG.

B. Heart Rate

The normal resting heart rate of a healthy human adult was traditionally defined as in the range of **[**60, 100**]** beats/min. Bradycardia (bellow 60 beats/min) and Tachycardia (above 100 beats/min) are considered pathological heart rates [15]. The range of possible heart rates is not straightforward to define. Athletes can show a resting heart beat as low as **[**30, 40**]** beats/min, which is known as athlete's heart syndrome [16]. The highest heart rate a human can achieve during excising, is strongly correlated with age. In young adults heart rates up to 220 beats/min were measured [17]. Given all this considerations, in conjunction with the filter limitations, this work is considering a range of **[**45, 200**]** beats/min.

III. Related Work

A. Contact PPG

PPG measurements with blue, red and near-IR lights are possible [18]. Different light wavelengths perform differently for different skin tones and situations (for example: measurements under motion). Smartphone and smartwatch manufacturers are also using PPG technology [19], [20]. Contact PPG is widely used in smartwatches to obtain the heart rate. For example, smartwatches as the Mio Alpha and forearm devices as Schosche Rhythm are using green or IR light to detect the pulse on the wrist and arm [19]. Jihyoung Lee and his team claim that green light gives best results in case of motions [18]. Typical devices for blood oxygen saturation measurements are using a combination of red and IR light due to the deep tissue penetration [21]. Many of these devices use the transmission plethysmography, *i.e.* emitter and detector are located opposite each other. In our approach we are using a ToF camera with reflective plethysmography, *i.e.* emitter and detector are on the same side [1]. Bone, various tissues, arterial and venous blood contribute amongst other influences in reflecting the emitted active IR illumination back into the ToF photodiodes [22]. Typical placements for measuring the pulse are the fingers, toes, wrist and ear lobes [23].

B. Remote PPG

In remote PPG the sensor is not attached to the subject but measures parts of the skin or the face remotely. A lot of research was done on extracting the heart rate from facial colour videos (rgbPPG). Extensive reviews on the used rgbPPG methods exist [24]–[26]. The reviews report methods using multi spectral, additional wavelengths such as orange and cyan [24], high quality cameras to consumer grade web cams [26]. The mentioned methods differ in the selection of regions of interest (ROI). The forehead, cheeks, lips and other parts up to the full face were tried as ROI [25]. In addition, methods for skin region selection in colour videos exist [26].

To reduce motion artefacts and noise and reconstruct the PPG signal more truthfully, many of the reported methods combine the colour channels. For combining the colour channels derived weighting schemes or blind source separation (BSS) were used. In the reviews mentioned BSS methods include versions of the Independent Component Analysis (ICA) or Principal Component Analysis (PCA). As another method of denoising, passband filters, stochastic filters and wavelet analysis are used, in combination with BSS or separate. Depending on the method, filters were applied before and after the colour channel combination. The heart rate was then derived either by peak extraction or by spectral density estimates such as fast Fourier transform (FFT) [26]. General video magnification algorithm were also suggested to be used to determine the heart rate [27], or amplify the signal before further processing [28]. A video magnification algorithm was used for real-time visualization of the heart rate on Microsoft Kinect camera data [29]. For extraction of the pulse wave rgbPPG is not limited to skin reflection changes in the video. It is shown that heart rate can be extracted from slight head movements due to the pressure variations in the carotid arteries [30]. However rgbPPG methods which rely on passive illumination, are prone to errors due to spatial and temporal illumination variations. Several approaches were evaluated to algorithmically improve the temporal illumination variation resistance of rgbPPG [24]–[26].

Nevertheless, methods that use passive illumination, will not work in the dark. Thermal cameras and IR cameras are known to work well in the dark. Methods using thermal cameras [31], thermal cameras in combination with IR cameras [32] and solely IR cameras have been used for remote heart rate estimation. An approach was presented which uses a single wavelength IR camera to estimate the heart rate in the face by spectrum analysis [33]. The benefit of rgbPPG is the availability of more than one wavelength to reduce noise by putting the different measurements into reference. A similar approach was explored by using three different IR wavelengths [34]. Remote pulse oxygenation measurement on the face is also demonstrated using orange and IR wavelengths [35]. It was further shown that real time remote PPG measurement with peak detection using an IR camera is possible on a FPGA [36]. The Microsoft Kinect RGBD camera has also been explored for its use in heart rate measurement. Several approaches utilize the RGB camera of the Kinect for this purpose. The dominant frequencies in the spectral density estimate are used to estimate the heart rate, which is not uncommon for remote PPG algorithm [37]–[39]. More heart rate estimation approaches were presented using the amplitude data of the Kinect depth camera and a spectral density estimate [40], [41]. As our approach aims at recovering the pulse peak locations, including N-N intervals, this heart rate estimation technique is not enough. Another method uses the head movement to extract the heart rate [42], but in comparison to rgbPPG methods the depth data is used for motion tracking. Our method also uses solely a depth camera, but in contrast, we utilize the amplitude data to track the skin absorption changes. Further methods where proposed which track the heart rate and the respiratory rate simultaneously. An early method required the subjects to lie down and expose the chest during measurement. The measurement regions included the carotid artery, however the regions were selected manually [43]. In contrast our method selects the region automatically and does not necessarily choose the carotid artery. A later approach estimated both vital signs simultaneously from a spectral density estimate [40]. One of the most recent methods tracks both vital signs using RGB or IR data, depending on the lightning conditions, for abnormality monitoring during sleep. In contrast to our method the vital sings are extracted from the abdominal-thoracic region which has to be visible. While we extract the heart rate from the head and throat.

IV. Method

In this section we will describe the contact and remote methods used to measure the pulse wave with a Pico Flexx ToF camera. This ToF camera uses the phase difference between pulsed IR light and its reflection to measure depth. To remove depth ambiguities, several phase shifted measurements (phases) are used. ToF cameras can operate on different use-case settings. A use-case setting consists of a predefined framerate, illumination time and number of phases used to calculate the depth and amplitude image. The quality of the signal improves with higher illumination time. However, if the phases or the illumination time go up, the framerate has to go down, to adhere the laser skin and eye safety requirements. Additionally it depends on the framerate how accurately a peak of the pulse wave can be sampled. Accurate sampling of the pulse peak is important for the calculation of the HRV. Therefore a trade-off between framerate and illumination time has to be found. For our experiments we have chosen to evaluate a framerate 45 frames per second and the maximal illumination time of 500 microseconds. With these settings, we trade a higher peak sampling accuracy for slightly more noise.

A. Contact PPG

The IR light of the ToF camera penetrates the tissue and is partially reflected and absorbed. The absorbed part of the light can be divided into two fractions, pulse independent absorption and the pulse dependent absorption. The first fraction is caused

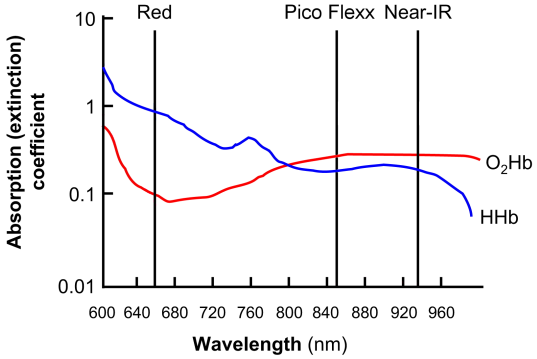

Fig. 2. Behaviour of oxygenated blood (O_2Hb) and oxygen depleted blood (HHb) under different wavelengths. Obtained with changes from [44].

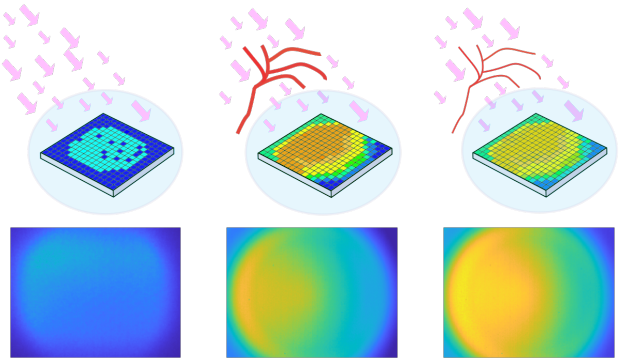

(a) (b) (c)

Fig. 3. Examples to demonstrate how the amplitude image changes without a finger (a), with a finger having an increased blood volume (b) and a finger having a decreased blood volume (c). Pseudo colours are used to highlight the amplitude intensity changes.

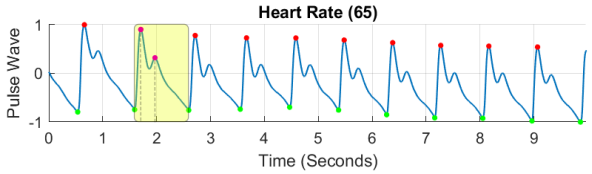

Fig. 4. Measurement with contact PPG over ten seconds. The yellow area highlights a single pulse cycle. Up to the first peak it is called systolic phase. The rest of the wave is the diastolic phase.

by the absorption of tissue, bone and venous blood [45]. This fraction has close to no variations and is disregarded. The second fraction varies, depending on whether a pulse has occurred or not. If a pulse takes place, the pulsating arterial blood absorbs more IR light, as the blood volume increases. Oxygenated blood absorbs more IR light than oxygen depleted blood at 850 nanometres wavelength. This absorption behaviour of different wavelengths is shown in Fig. 2. Because of this effect we have inverted the signal and now consider the high points instead low points as it is more intuitive. Fig. 3 shows how the light is reflected from the vessels and bones in a human finger. For better visualization we use a pseudo colouring scheme to make the intensity changes better visible. In (a) the amplitude image without a finger is illustrated. In (b) and (c) a finger is placed on the camera and covers the whole sensor. A pulse with fresh, oxygen enriched blood from the heart causes a higher blood volume in the arteries, which results in increased absorption. More absorption means that less light is reflected and arrives at the sensor, which results in a darker image. When the oxygen depleted blood volume lowers at the end of the pulse cycle, less IR light is absorbed, which results in a slightly brighter image.

As our ToF camera is limited to reflective PPG, the tissue has to be placed right on top of the illumination unit and the receiver. Important for good results is a complete coverage of the receiver with the tissue. Several body locations were tested, and several possible placements were found. As reported in literature, a good signal was found in body parts such as toes, fingers and ear lobes. However, it was found to be the most stable configuration to use one finger to cover both, the illumination unit and the receiver. The finger has a rich arterial blood supply and the sensor can be fixated with relative ease, which supports to reduce motion errors. We are using the ToF amplitude data for our method. It can be described as a grayscale image that is derived from the active IR illumination and independent of passive illumination.

Given the amplitude image, the pulse wave is calculated as the mean intensity of all pixels in every frame. The result of a 10 seconds lasting measurement is illustrated in Fig. 4. The pulse wave is centred as the absolute intensity values are less important for heart rate and PRV analysis as the relative changes at each time stamp. The ECG heart beat intervals are similar to the peak distances of the pulse wave. The AHR, SDNN and CV_{PRV} can be derived from the pulse wave. To calculate these measures, the peaks need to be detected in the pulse wave.

B. Peak Detection

The yellow area in Fig. 4 highlights a single pulse cycle. The first part of the signal up to the first line is the systolic phase. The rest is part of the diastolic phase [46]. It can be seen that the pulse cycle has two characteristic peaks, the first and most prominent in the systolic phase and the second smaller one in the diastolic phase. Only the peak of the systolic phase is used for the calculation of AHR, SDNN and CV_{PRV}. To suppress the peak of the diastolic phase, an empirically determined factor of 0.4 is multiplied to the average peak high of the systolic phase. This determines the threshold for the final peak detection. In most cases, the small peaks of the diastolic phase, will not reach 40% of the height of a systolic peak.

Within the first run over the whole signal, the potential high points are marked which passes the threshold. For a more stable detection also a threshold on time stamps is used. Each incoming frame has time stamp. Within a second run over the signal, an arithmetic mean value $\overline{\Delta^t}_{temp}$ is calculated over all delta time stamps

$$\Delta_i^t = t_{i+1} - t_i, \tag{4}$$

where t_i is the time of the current peak and t_{i+1} of the next peak. With this temporal mean value and the dynamic amplitude threshold, we sort out unwanted peaks in our PPG signal. The time difference between the last peak and the new potential peak must be at least 60% of the temporal mean value. After sorting out unwanted peaks, the real mean value ($\overline{\Delta^t}$) can be calculated from the remaining peaks. With the remaining peaks and the corresponding time stamps, the AHR, SDNN and CV_{PRV} are calculated. The equations for these quantitative measures are given in Section II. Once the pulse wave is extracted with the remote PPG method the same detection can be applied and the measurement values calculated.

C. Remote PPG

In order to extract the pulse wave from a ToF amplitude video of a subject's face, a multi-step process is used. The amplitude data contains regions in which a pulse wave can be located. These regions consist of subsections on the human

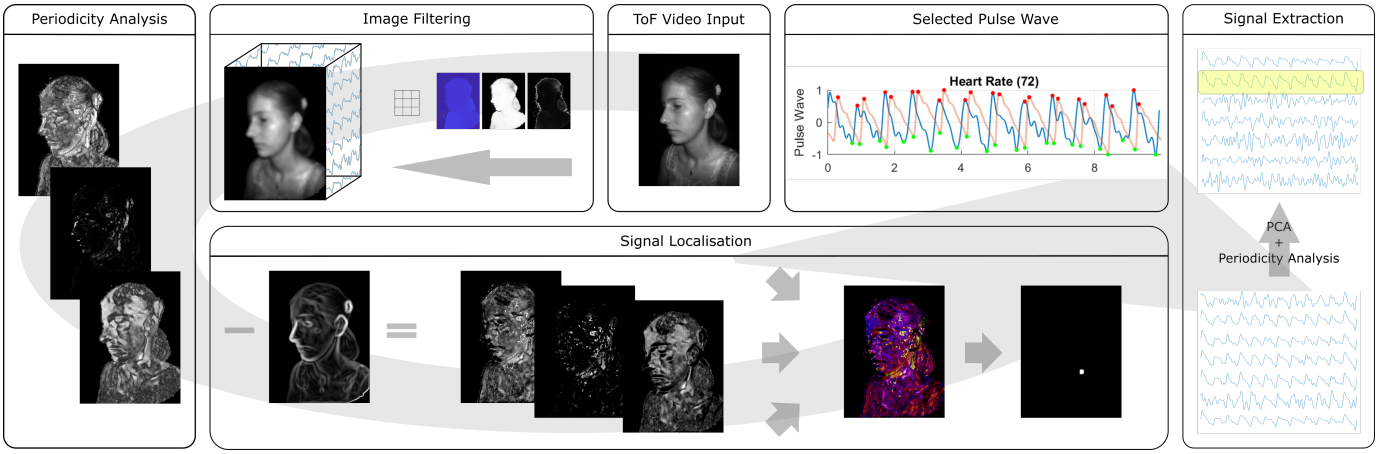

Fig. 5. Sample pipeline of the remote PPG signal extraction algorithm. The input consist of a ToF video and will be spatially pre-filtered to remove the background and camera noise. For the extraction of the pulse wave the amplitude data will be used. Every pixel in the pre-filtered video will be regarded as a signal over time and analysed for its potential to contain a pulse wave. Periodicity and pulse wave shape characteristics are used to create three heat maps. By edge suppression, energy equalization followed by combining of the three heat maps, one heat map is created. By thresholding and iterative adjustment of the threshold, the final mask is extracted. The signal is recovered by BSS or averaging. The final pulse wave is selected by periodicity and pulse wave shape characteristics analysis.

skin but not the whole. It can be explained by light absorption properties being skin region dependent [47]. By considering every pixel in the video to be a signal over time and analysing it for its potential to contain a sufficiently clear pulse wave, a mask is created. The analysis is based on signal periodicity and pulse wave shape characteristics. Passband signal filtering is used to limit the influence of noise and movement artefacts. This calculated mask is used for signal localisation and the selection of a subset of time series for further processing. To recover the pulse wave from the bundle of selected signals, BSS is used. As the best pulse signal does not need to be contained in the first component, the signal with the highest score on signal periodicity and pulse wave shape characteristics, is selected for peak detection and heart rate calculation. A summary of the algorithms pipeline is shown in Fig. 5.

1) Image Filtering: To counteract the inherently noisy ToF image, spatial filtering is used. The box filter with a kernel size of 5x5 was selected. To reduce calculation time, the ToF depth, noise and confidence data is used to pre-filter the video. The noise and confidence data is used to filter the frames for regions with high confidence and low noise. Additionally the median of the depth value of all non-zero measurements is calculated and half a meter around is selected to be the subject. This simplification is justified by the requirement that the subject has to be close enough to the ToF camera to fill most of the image. Alternatively, face detection could be used to determine the average position of the subject.

2) Signal Filtering: As previously discussed, PPG is very prone to motion errors. To further reduce sensor noise and motion influences, temporal filtering will be used to improve the signal. As discussed in Section II, the heart rate range of interest is limited to [45, 200] beats/min which translates to [0.75, 3] Hz. In [30], it is mentioned that frequencies lower than 0.75 Hz negatively affect the algorithm. It was observed, that those frequencies tend to correlate with slow

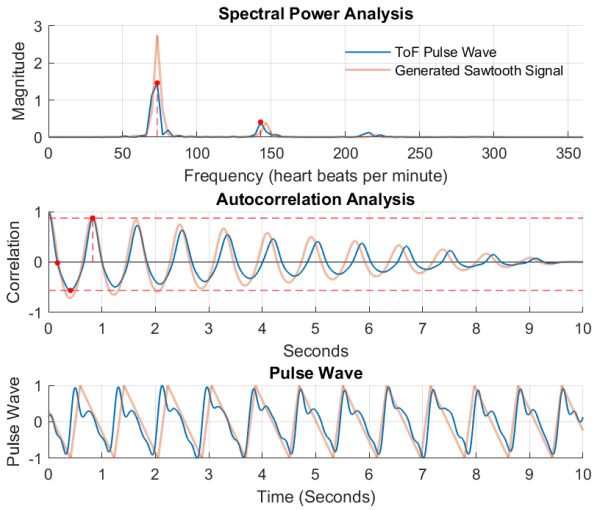

Fig. 6. Periodicity analysis of a passband filtered contact PPG pulse wave and comparison to a sawtooth signal with same average peak width. The upper plot visualizes the analysis by autocorrelation. The middle plot visualizes the analysis with the spectral power density estimate. The lowest plot shows the reference pulse wave and sawtooth signal.

movements of the subject, such as breathing. It is further suggested to choose a passband in the range of [0.75, 5] Hz as higher frequencies contain information needed for peak detection [30]. Given this argument it was decided to filter with an ideal filter and a passband of [0.75, 5].

3) Signal Periodicity Analysis: For final pulse wave selection and pulse localisation analysis, the signals are analysed for certain properties. One property is periodicity. A measure for periodicity is calculated, by using the autocorrelation function. To reduce the function to one descriptive value the maximum value after the first zero crossing is selected. When further analysing the pulse wave, a similarity to a sawtooth signal can be seen. For these kinds of signals, a strong frequency response at several harmonic positions is characteristic. Due

to this property, the energy contained in the main frequency component and its second harmonic, is used as a measure for a pulse wave like signal [30], [42]. Two derived descriptive values are used, once this contained energy is put into relation to the overall contained peak energies, and once into relation of the rest of the peak energies. It has to be noted that, in order for both analysis to give good results, it is best to centre the signal and filter out low, movement related, frequencies. A visualisation of the analysis principle on a passband filtered contact PPG pulse wave, in comparison to an artificial sawtooth signal, can be seen in Fig. 6.

4) Signal Localisation: As it is not a sufficient approach to select all or random parts of the subject's skin, a pulse wave signal localisation analysis is performed. As mentioned before, every pixel in the video is considered to be a signal over time. The signal periodicity analysis metrics are used to create three heat maps. An example of the heat maps can be seen in Fig. 5. A strong false positive response of the heat maps was observed near edge regions. These regions are prone to strong changes even due to slight motion. To suppress this error source the Sobel gradient of the mean image is subtracted from the heat maps. Before edge suppression and combining of the heat maps, the energy contained in every heat map is adjusted to be distributed around the mean. As the used metrics will also respond to other signals than the pulse wave, all three resulting heat maps are used as a way of false positive suppression. The combined heat maps are thresholded to create the final mask. To remove outliers from the heat maps, a median filter is used before thresholding. To further address the problem of threshold choice, a threshold of 95% is applied, and lowered gradually until at least the required number of pixels was selected, even after minor components were cleared from the masks by morphological operations. The number of required pixels is the number of desired components to be extracted by the BSS. This results in the best region being accepted as final mask.

5) Signal Extraction: Even after region selection and pre-filtering to the range of intended frequencies, the signal is not necessarily clear enough to be extracted directly by averaging the selected signals. To recovery the pulse wave from the noisy signals BSS is used. As BSS algorithm, PCA was selected. However cases were observed in which the signal was clearly recovered by averaging the selected signals, while BSS failed. In other cases it was observed that with only the average, no pulse wave could be extracted, while BSS was able to recover it. In most cases of a successful extraction, the signal was observed to be contained in the first four components. As the pulse wave is not always contained in the first component, the previously explained signal periodicity analysis metrics are used to select the best pulse wave. It was decided to regard the first six components as potential pulse waves. In order to address the previously described problem the average of the selected signals is included in the pool of potential pulse waves. This emphasises the need for post selection of the signal with the highest score on periodicity and pulse wave shape characteristics. The BSS algorithm happens to extract the correct and sometimes the inverted pulse wave. Prior to peak detection and heart rate calculation the selected signal is analysed for its characteristic pulse wave shape. If the inverted signal scores higher it is selected as the final pulse wave.

V. Results

Both approaches were designed in Matlab, while the contact PPG approach was ported to Android. Also the designed remote PPG method can be migrated to other platforms. Results for both methods are provided in this section. The tested ToF camera is a Pico Flexx model of PMD Technologies AG. To show the accuracy of our methods AHR, SDNN and CV_{PRV} are used as a measure. Contact and remote PPG are very sensitive to motion. Therefore the test subjects were asked to remain relatively still while the measurements were taken.

For the contact PPG experiments the ToF camera is mounted on the finger of the subject. Note that it is important not to attach the sensor too firmly to the subjects finger, as pressure influences the measurement. We use eight recordings of seven subjects. The selected test subjects consisted of four males and three females. The measurement was taken for an average of one minute. As a reference the Polar H7 chest belt (with ECG quality) and a pulse oximeter PO-250 from Pulox is used. In Fig. 7 a comparison of a ToF pulse wave and a pulse oximeter wave is given. It can be seen that the curves are a close match. However for detailed evaluation in regard to AHR, SDNN and CV_{HRV} only the Polar H7 chest belt is used as a reference.

For the remote PPG experiments we evaluate a total of eighteen recordings. The selected test subjects consisted of four males and four females. An additional limitation for remote PPG is, that the subjects need to remain close to the camera, in a range of about 30cm to 40cm. An additional limitation in relation to background illumination, such as sunlight, was not found to be necessary. This can be explained by the close distance to the sensor and the background illumination suppressing properties of this ToF measurement principle. The measurements are recorded for ten seconds, simultaneously with two ToF cameras. One ToF camera records the face, another ToF camera is securely mounted on the finger. The IR light source of the second ToF camera is completely covered by the finger, therefore interference between the ToF cameras is not to be expected. The finger mounted ToF camera is used to provide a ground truth pulse wave. The choice of the reference measurement is based on several factors. As the same light wavelength is used, the pulse wave signal appearance is expected to be similar. For evaluation of pulse wave form extraction quality we intended to utilize a sensor

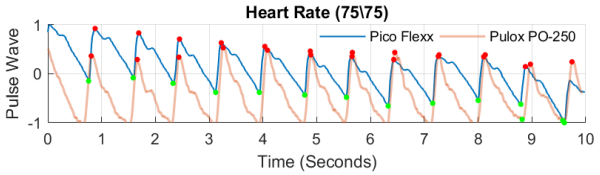

Fig. 7. Comparison between pulse oximeter and ToF camera over 10 seconds. The orange line shows the result of the pulse oximeter, the blue line shows the ToF signal.

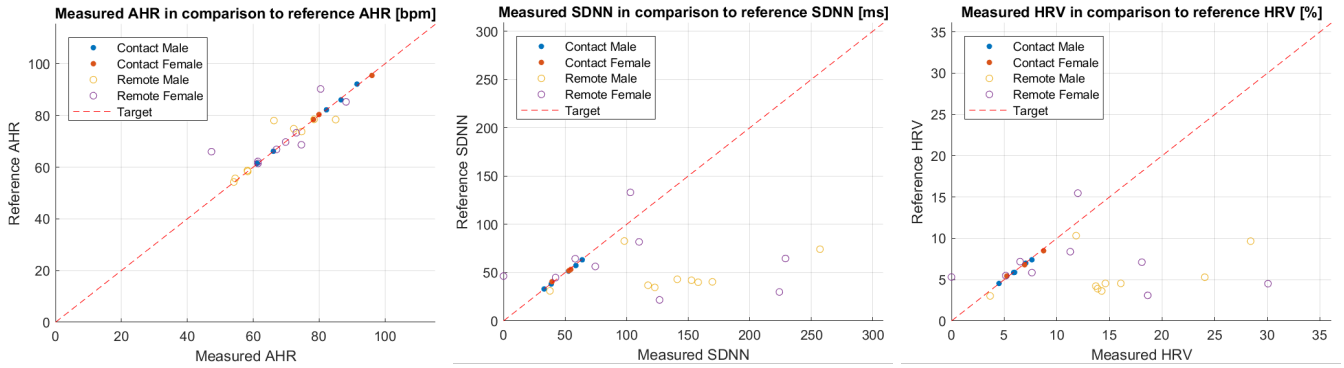

(a) AHR Error. (b) SDNN Error. (c) PRV Error.

Fig. 8. The comparison of the measured AHR, SDNN and PRV in relation to their selected reference measurement.

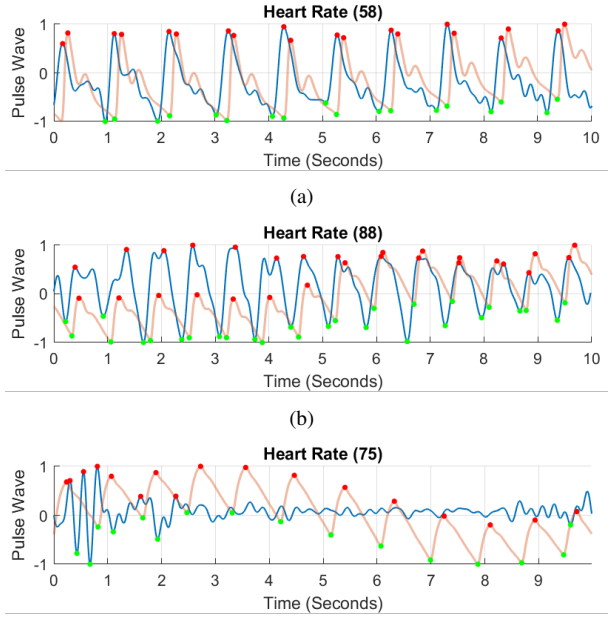

(a)

(b)

(c)

Fig. 9. Examples of three remote pulse waves (blue) in comparison to contact pulse waves (orange). Depending on quality, the results are sorted into three categories. In (a) good quality and in (b) medium quality wave is shown. In (c) an example of a failure case is given.

providing a reference pulse wave, which the Polar H7 chest belt does not simply provide. Additionally good accuracy of the contact PPG method in reference to the provided measurements of the chest belt, was shown. Good results were achieved when analysing the amplitude data. For the sake of understanding we categorized the results into three categories, good quality, medium quality and failure case. In the test set seven samples were selected to be good quality, eight more to be medium quality and three failure cases. An example of the three different quality stages is shown in Fig. 9. The results show that an accurate heart rate can be extracted from the good and medium quality signal. While mesures derived from the PRV suffer much sooner from inaccuracies and also medium quality signals will not provide sufficient results.

A detailed plot of the results for both methods is given in Fig. 8. The average error and standard deviation, is given in

TABLE I
AVERAGE (AVG.) ERROR AND STANDARD DEVIATION (SD) OF THE ERROR

	contact PPG		remote PPG	
Error	**Avg.**	**SD**	**Avg.**	**SD**
AHR [BPM]	0.33	0.26	3.46	5.22
SDNN [ms]	0.95	0.46	79.15	63.08
CV_{HRV} **[%]**	0.13	0.09	8.77	7.37

Table I. From the quantitative measurements it can be seen that the quality of the contact PPG method is sufficient for personal assistance applications. However the remote PPG method still requires improvements in the areas of motion resistance and pulse peak extraction. Especially the PRV measures derived from the remote PPG signals are currently still quite erroneous and require improvement in the temporal peak location extraction. From the results it can be seen that the pulse wave is a lot harder to extract from remote ToF data, than from contact data. The pulse wave cannot be found in every part of the exposed skin. It is argued that several factors may influence the signal to noise ration. Factors found to have an influence are, the distance to the camera, the incident angle on the skin, the exposed skin regions and the skin of the subject itself even amongst subjects with similar skin colour. A difference in light wavelengths efficiency in rgbPPG in relation to different skin colours was reported [48]. However it was suggested that differences in optical properties can even be subject dependent or temperature related [49]. To the best of our knowledge no study exists which examines the differences in remote PPG response between subjects of the same skin colour. Further research is needed. Additionally, it can be observed that, depending on the strength of the N-N interval variations the spectral power analysis may display more than one major frequency peak. This leads to a less discriminative results, while the autocorrelation is not as strongly affected. Nevertheless, in case the signal localisation or pulse wave selection fails, it can either be that no signal was found in the subjects skin or periodicity analysis failed in favour of other periodic movements such as repeated swallowing or hair moment in the wind.

In fifteen out of eighteen measurements, the method was observed to be able to localise a clear enough signal. The

method works best, if one carotid artery is exposed, as can be seen Fig. 1. However, signal localisation analysis was observed to find a signal up until the superficial temporal artery and also in the cheeks and the forehead.

VI. Summary

This paper has explored the use of a Pico Flexx ToF camera of PMD Technologies AG for contact and remote PPG. Two methods are introduced, to successfully measure the human heart rate with contact and remote PPG. Contact PPG further shows high accuracy in respect to HRV measures. Our findings show that contact and remote PPG on a ToF camera are feasible but also very sensitive to motion. For remote PPG, an additional limitation is that the subjects need to remain close to the camera. It is shown that it works best if one carotid artery is exposed, but the approach is not limited to it. One of the largest benefits of IR base PPG methods is the usability in the dark without the need of visible light. This qualifies the method to be used for night time driver monitoring and sleep monitoring. Improvements that we may address in future work include the increase of motion robustness, either in the described method or in a derived method. We further intend to explore different approaches for calculating the PRV measures, which are less susceptible to small errors in the remote measurement. Additionally, we aim at a subsequent study with a larger number of subjects including different skin tones and an evaluation of processing time.

Acknowledgments

The authors would like to thank the European Commission and its Horizon 2020 program, which funded the TrustVehicle project under the grant agreement n° 723324.

References

[1] K. H. Shelley, "Photoplethysmography: Beyond the Calculation of Arterial Oxygen Saturation and Heart Rate," *Anesth. Analg.*, vol. 105, no. 6, pp. 31–36, Dec. 2007.

[2] A. B. Hertzman, "Photoelectric Plethysmography of the Fingers and Toes in Man," *Proc. Soc. Exp. Biol. Med.*, vol. 37, no. 3, pp. 529–534, Dec. 1937.

[3] W. Verkruysse, L. O. Svaasand, and J. S. Nelson, "Remote plethysmographic imaging using ambient light." *Opt. Express*, vol. 16, no. 26, pp. 21 434–21 445, Dec. 2008.

[4] F. P. Wieringa, F. Mastik, and A. F. van der Steen, "Contactless multiple wavelength photoplethysmographic imaging: a first step toward SpO 2 camera technology," *Ann. Biomed. Eng.*, vol. 33, no. 8, pp. 1034–1041, Aug. 2005.

[5] R. Zangrniz, A. Martnez-Rodrigo, M. T. Lpez, J. M. Pastor, and A. Fernndez-Caballero, "Estimation of Mental Distress from Photoplethysmography," *Appl. Sci.*, vol. 8, no. 1, p. 69, Jan. 2018.

[6] G. Li and W.-Y. Chung, "Detection of Driver Drowsiness Using Wavelet Analysis of Heart Rate Variability and a Support Vector Machine Classifier," *Sensors*, vol. 13, no. 12, pp. 16 494–16 511, Dec. 2013.

[7] F. Shaffer and J. P. Ginsberg, "An overview of heart rate variability metrics and norms," *Frontiers in Public Health*, vol. 5, p. 258, 2017.

[8] H. Park, S. Oh, and M. Hahn, "Drowsy Driving Detection Based on Human Pulse Wave by Photoplethysmography Signal Processing," in *Proc. 3rd Int. Univer. Commun. Symp.*, Dec. 2009, pp. 89–92.

[9] M.-C. Li and Y.-H. Lin, "A real-time non-contact pulse rate detector based on smartphone," in *International Symposium on Next-Generation Electronics (ISNE)*. IEEE, May 2015, pp. 1–3.

[10] D. McDuff, C. Hurter, and M. Gonzalez-Franco, "Pulse and Vital Sign Measurement in Mixed Reality Using a HoloLens," in *Proc. ACM Symp. Virtual Real. Softw. Technol.* ACM, Nov. 2017, pp. 34:1–34:9.

[11] V. Jeyhani, S. Mahdiani, M. Peltokangas, and A. Vehkaoja, "Comparison of hrv parameters derived from photoplethysmography and electrocardiography signals," in *Conf. Proc. IEEE Eng. Med. Biol. Soc.*, Aug. 2015, pp. 5952–5955.

[12] M. Elgendi, "On the Analysis of Fingertip Photoplethysmogram Signals," *Curr. Cardiol. Rev.*, vol. 8, no. 1, pp. 14–25, Feb. 2012.

[13] G. Lu and F. Yang, "Limitations of oximetry to measure heart rate variability measures," *Cardiovasc. Eng.*, vol. 9, no. 3, pp. 119–125, 2009.

[14] N. Pinheiro, R. Couceiro, J. Henriques, J. Muehlsteff, I. Quintal, L. Gonçalves, and P. Carvalho, "Can PPG be used for HRV analysis?" in *Conf. Proc. IEEE Eng. Med. Biol. Soc.*, Aug. 2016, pp. 2945–2949.

[15] P. Babington, *Praktische Elektrokardiographie und Elektrophysiologie des Herzens: ein diagnostischer und therapeutischer Leitfaden für Studenten und Ärzte*, 1st ed. Stuttgart: Gustav Fischer, 1988.

[16] W. Micheo, E. Amy, and J. Correa, "Laboratory Tests and Diagnostic Imaging," in *Clinical Sports Medicine: Medical Management and Rehabilitation*, Frontera, Walter R. and Herring, Stanley A. and Micheli, Lyle J. and Silver, Julie K. and Young, Timothy P., Ed. Saunders, Philadelphia, PA, 2007, pp. 187–191.

[17] H. Tanaka, K. D. Monahan, and D. R. Seals, "Age-predicted maximal heart rate revisited," *J. Am. Coll. Cardiol.*, vol. 37, no. 1, pp. 153–156, Jan. 2001.

[18] J. Lee, K. Matsumura, K.-i. Yamakoshi, P. Rolfe, S. Tanaka, and T. Yamakoshi, "Comparison between red, green and blue light reflection photoplethysmography for heart rate monitoring during motion," in *Conf. Proc. IEEE Eng. Med. Biol. Soc.*, Jul. 2013, pp. 1724–1727.

[19] J. Parak and I. Korhonen, "Evaluation of wearable consumer heart rate monitors based on photopletysmography," in *Conf. Proc. IEEE Eng. Med. Biol. Soc.*, Aug. 2014, pp. 3670–3673.

[20] D. Grimaldi, Y. Kurylyak, F. Lamonaca, and A. Nastro, "Photoplethysmography detection by smartphone's videocamera," in *IEEE International Conference on Intelligent Data Acquisition and Advanced Computing Systems (IDAACS)*, vol. 1, Sep. 2011, pp. 488–491.

[21] J. Liu, B. P.-Y. Yan, W.-X. Dai, X.-R. Ding, Y.-T. Zhang, and N. Zhao, "Multi-wavelength photoplethysmography method for skin arterial pulse extraction," *Biomed. Opt. Express*, vol. 7, no. 10, pp. 4313–4326, 2016.

[22] N. Constant, T. Wang, and K. Mankodiya, "Pulseband: A hands-on tutorial on how to design a smart wristband to monitor heart-rate," in *IEEE Virtual Conference on Applications of Commercial Sensors (VCACS)*, Mar. 2015, pp. 1–3.

[23] Y. Sun and N. Thakor, "Photoplethysmography revisited: from contact to noncontact, from point to imaging," *IEEE Trans. Biomed. Eng.*, vol. 63, no. 3, pp. 463–477, Mar. 2016.

[24] D. J. McDuff, J. R. Estepp, A. M. Piasecki, and E. B. Blackford, "A survey of remote optical photoplethysmographic imaging methods," in *Conf. Proc. IEEE Eng. Med. Biol. Soc.*, Aug. 2015, pp. 6398–6404.

[25] M. Hassan, A. Malik, D. Fofi, N. Saad, B. Karasfi, Y. Ali, and F. Meriaudeau, "Heart rate estimation using facial video: A review," *Biomed. Signal Process. Control.*, vol. 38, pp. 346–360, Sep. 2017.

[26] P. V. Rouast, M. T. P. Adam, R. Chiong, D. Cornforth, and E. Lux, "Remote heart rate measurement using low-cost RGB face video: a technical literature review," *Front. Comput. Sci.*, Dec. 2017.

[27] H.-Y. Wu, M. Rubinstein, E. Shih, J. Guttag, F. Durand, and W. T. Freeman, "Eulerian Video Magnification for Revealing Subtle Changes in the World," *ACM Trans. Graph*, vol. 31, no. 4, pp. 1–8, Jul. 2012.

[28] A. Al-Naji and J. Chahl, "Detection of Cardiopulmonary Activity and Related Abnormal Events Using Microsoft Kinect Sensor," *Sensors*, vol. 18, no. 3, p. 920, Mar. 2018.

[29] T. Smilkstein, M. Buenrostro, A. Kenyon, M. Lienemann, and G. Larson, "Heart rate monitoring using Kinect and color amplification," in *Proc. IEEE Healthcare Innovation Conf. (HIC)*. IEEE, Oct. 2014, pp. 60–62.

[30] G. Balakrishnan, F. Durand, and J. Guttag, "Detecting Pulse from Head Motions in Video," in *Proc. IEEE Comput. Soc. Conf. Comput. Vis. Pattern. Recognit.*, Jun. 2013, pp. 3430–3437.

[31] M. Garbey, N. Sun, A. Merla, and I. Pavlidis, "Contact-Free Measurement of Cardiac Pulse Based on the Analysis of Thermal Imagery," *IEEE Trans. Biomed. Eng.*, vol. 54, no. 8, pp. 1418–1426, Aug. 2007.

[32] M. Hu, G. Zhai, D. Li, Y. Fan, H. Duan, W. Zhu, and X. Yang, "Combination of near-infrared and thermal imaging techniques for the remote and simultaneous measurements of breathing and heart rates under sleep situation," *PloS one*, vol. 13, no. 1, pp. 1–14, Jan. 2018.

[33] M. Lindelw and A. Lindqvist, "Remote heart rate extraction from near infrared videos - An approach to heart rate measurements for the smart eye head tracking system," M.S. Thesis, Department of Signals and Systems, Chalmers University of Technology, Gteborg, 2016.

[34] M. van Gastel, S. Stuijk, and G. de Haan, "Motion Robust Remote-PPG in Infrared," *IEEE Trans. Biomed. Eng.*, vol. 62, no. 5, pp. 1425–1433, May 2015.

[35] D. Shao, C. Liu, F. Tsow, Y. Yang, Z. Du, R. Iriya, H. Yu, and N. Tao, "Noncontact Monitoring of Blood Oxygen Saturation Using Camera and Dual-Wavelength Imaging System," *IEEE Trans. Biomed. Eng.*, vol. 63, no. 6, pp. 1091–1098, Jun. 2016.

[36] Y.-C. Lin, N.-K. Chou, G.-Y. Lin, M.-H. Li, and Y.-H. Lin, "A Real-Time Contactless Pulse Rate and Motion Status Monitoring System Based on Complexion Tracking," *Sensors*, vol. 17, no. 7, 2017.

[37] I. Bosi, C. Cogerino, and M. Bazzani, "Real-time monitoring of heart rate by processing of Microsoft Kinect 2.0 generated streams," in *International Multidisciplinary Conference on Computer and Energy Science (SpliTech)*, Jul. 2016.

[38] L. Zhou, M. Yin, X. Xu, X. Yuan, and X. Liu, "Non-contact detection of human heart rate with Kinect," *Cluster Comput.*, pp. 1–8, Jan. 2018.

[39] E. Gambi, A. Agostinelli, A. Belli, L. Burattini, E. Cippitelli, S. Fioretti, P. Pierleoni, M. Ricciuti, A. Sbrollini, and S. Spinsante, "Heart Rate Detection Using Microsoft Kinect: Validation and Comparison to Wearable Devices," *Sensors*, vol. 17, no. 8, p. 1776, Aug. 2017.

[40] A. Procházka, M. Schätz, O. Vyšata, and M. Vališ, "Microsoft kinect visual and depth sensors for breathing and heart rate analysis," *Sensors*, vol. 16, no. 7, p. 996, Jun. 2016.

[41] I. Bosi, C. Cogerino, and M. Bazzani. (2017, June) *Real-Time Monitoring of Heart Rate by Processing of Near Infrared Generated Streams*. Accessed on: Apr. 03, 2018. [Online]. Available: https://www.researchgate.net/publication/318402304_Real-Time_Monitoring_of_Heart_Rate_by_Processing_of_Near_Infrared_Generated_Streams

[42] C. Yang, G. Cheung, and V. Stankovic, "Estimating Heart Rate and Rhythm via 3D Motion Tracking in Depth Video," *IEEE Trans. Multimedia*, vol. 19, no. 7, pp. 1625–1636, Jul. 2017.

[43] N. Bernacchia, L. Scalise, L. Casacanditella, I. Ercoli, P. Marchionni, and E. P. Tomasini, "Non contact measurement of heart and respiration rates based on kinect," in *IEEE Int. Symp. Med. Meas. Appl.*, Jun. 2014, pp. 1–5.

[44] E. D. Chan, M. M. Chan, and M. M. Chan, "Pulse oximetry: understanding its basic principles facilitates appreciation of its limitations," *Respir. Med.*, vol. 107, no. 6, pp. 789–799, 2013.

[45] T. Tamura, Y. Maeda, M. Sekine, and M. Yoshida, "Wearable Photoplethysmographic SensorsPast and Present," *Electronics*, vol. 3, no. 2, pp. 282–302, 2014.

[46] B. M. Jayadevappa and M. S. Holi, "Photoplethysmography: Design, Development, Analysis and Applications in Clinical and Physiological Measurement - A Review," *Int. j. innov. res. sci. eng. technol.*, vol. 5, no. 3, Mar. 2016.

[47] A. V. Moço, S. Stuijk, and G. de Haan, "Skin inhomogeneity as a source of error in remote ppg-imaging," *Biomed. Opt. Express*, vol. 7, no. 11, pp. 4718–4733, Nov. 2016.

[48] A. Królak, "Influence of Skin Tone on Efficiency of Vision-Based Heart Rate Estimation," in *Polish Conference on Biocybernetics and Biomedical Engineering*. Springer, Aug. 2017, pp. 44–55.

[49] T. Lister, P. A. Wright, and P. H. Chappell, "Optical properties of human skin," *J. Biomed. Opt.*, vol. 17, no. 9, pp. 1–14, 2012.